Mon. Not. R. Astron. Soc. **000**, 1–9 (2014) Printed 12 March 2014 (MN LATEX style file v2.2)

Chemical abundance analysis of symbiotic giants. I. RW Hya and SY Mus

Joanna Mikołajewska[1⋆], Cezary Gałan[1], Kenneth H. Hinkle[2], Mariusz Gromadzki[3], and Mirosław R. Schmidt[4]

[1]*N. Copernicus Astronomical Center, Bartycka 18, PL-00-716 Warsaw, Poland*
[2]*National Optical Astronomy Observatory, P.O. Box 26732, Tucson, AZ 85726, USA*
[3]*Departamento de Física y Astronomía, Universidad de Valparaíso, Av. Gran Bretaña 1111, Playa Ancha, Casilla 5030, Chile*
[4]*N. Copernicus Astronomical Center, Rabiańska 8, PL-87-100 Toruń, Poland*

arXiv:1403.2659v1 [astro-ph.SR] 11 Mar 2014

Accepted 2014 March 11 Received 2014 February 6

ABSTRACT

The study of symbiotic systems is of considerable importance in our understanding of binary system stellar evolution in systems where mass loss or transfer takes place. Elemental abundances are of special significance since they can be used to track mass exchange. However, there are few symbiotic giants for which the abundances are fairly well determined. Here we present for the first time a detailed analysis of the chemical composition for the giants in the RW Hya and SY Mus systems. The analysis is based on high resolution (R ~ 50000), high S/N, near-IR spectra. Spectrum synthesis employing standard LTE analysis and atmosphere models was used to obtain photospheric abundances of CNO and elements around the iron peak (Sc, Ti, Fe, and Ni). Our analysis reveals a significantly sub-solar metallicity, [Fe/H]~-0.75, for the RW Hya giant confirming its membership in the Galactic halo population and a near-solar metallicity for the SY Mus giant. The very low $^{12}C/^{13}C$ isotopic ratios, ~6–10, derived for both objects indicate that the giants have experienced the first dredge-up.

Key words: binaries: symbiotic – stars: abundances – stars: atmospheres – stars: late-type – stars: individual: RW Hya, SY Mus – stars: late-type

1 INTRODUCTION

Binary systems are an invaluable source of knowledge of the physical parameters of the stars. During some stage of stellar evolution most binary stellar systems undergo interactions between the components. The interactions turn on and off at various evolutionary stages, depending on the separation of components. Among the most interesting examples of such systems are the symbiotic systems. These are still often called symbiotic stars because their binary nature which we now consider obvious was controversial only thirty years ago.

Symbiotic systems are long-period interacting binaries in which an evolved giant transfers material to a hot and luminous companion surrounded by an ionized nebula. The hot component of the vast majority of symbiotic systems is a white dwarf (WD) although in two cases, V2116 Oph (Davidsen et al. 1977) and V934 Her (Garcia et al. 1983), a neutron star has been found. There are two distinct classes of symbiotic binaries. The S-type (stellar) have normal red giants and orbital periods in the range ~1–15 years. The D-type (dusty) have Mira primaries usually surrounded by a warm dust shell and orbital periods of typically decades to centuries. Mass exchange is the property that defines the symbiotic class. Even in the D-type systems the components are still close enough to allow the WDs to accrete material from the giant's stellar wind. Symbiotic systems are the interacting binaries with the longest orbital periods. Their study is essential to understand the evolution and interaction of detached and semi-detached binary stars.

The rich and luminous circumstellar environment surrounding the interacting symbiotic stellar members results from the presence of both an evolved giant with a heavy mass loss and a hot companion copious in ionizing photons often producing its own wind. The cool giant and the hot dwarf produce strongly different environments such as ionized and neutral regions, dust forming region(s), accretion/excretion disks, interacting winds, bipolar outflows, and jets. Such a complex multi-component structure makes symbiotic stars a very attractive laboratory to study many aspects of stellar evolution in binary systems. Firming links between symbiotic systems and related objects are essential to the understanding, for instance, of the role of interacting binaries in the formation of stellar jets, planetary nebulae, novae, supersoft X-ray sources (SSXS), and supernovae type Ia (SN Ia). Many of these issues concerning the late stages of stellar evolution are presently poorly understood but have important implications on our understanding of the stellar

⋆ E-mail: mikolaj@camk.edu.pl

© 2014 RAS

Table 1. Parameters of RW Hya and SY Mus

Parameter	RW Hya	SY Mus	Reference
$P_{\rm orb}$	370.2 days	625 days	Kenyon & Mikołajewska (1995) Dumm et al. (1998)
Sp Type	M2	M5	Belczyński et al. (2000)
$M_{\rm cool}$	1.6±0.3	1.30±0.25	Rutkowski et al. (2007)
$M_{\rm hot}$	0.48±0.06	0.43±0.05	Rutkowski et al. (2007)
$R_{\rm cool}$	122 $R_\odot$	135 $R_\odot$	Rutkowski et al. (2007)

Table 2. Journal of spectroscopic observations

Object	Band	Date	HJD(mid)	Orbital phase [a]
RW Hya	*H*	16.02.2003	2452686.8380	0.57
	K	20.04.2003	2452749.6295	0.74
	K	13.12.2003	2452986.8656	0.38
	K_r	03.04.2006	2453828.6308	0.65
SY Mus	*H*	17.02.2003	2452687.7566	0.02
	K	20.04.2003	2452749.5817	0.12
	K	13.12.2003	2452986.8250	0.50
	K_r	03.04.2006	2453828.5767	0.84

[a] Orbital phases calculated for RW Hya from orbital ephemerides of Kenyon & Mikołajewska (1995) or Schild et al. (1996) and for SY Mus from orbital ephemerides of Dumm et al. (1998)

population and chemical evolution of galaxies as well as the extragalactic distance scale.

Chemical composition is one of the major parameters along with initial mass that determine stellar evolution. Chemical composition has a strong influence on many important astrophysical processes. In the case of symbiotic stars it is generally believed that the symbiotic appearance and activity is triggered by high mass-loss rate of the giant (see e.g. Mikołajewska 2003, and references therein) possibly due to its enhanced metallicity (Jorissen 2003).

The apparent deficit of extrinsic C or S stars, i.e. cool components polluted by the s-process and C-rich material from the former TP-AGB companion, is among the most interesting problems raised by the S-type symbiotic binaries. There are other red giant – white dwarf binary star families with abundance peculiarities, for instance the barium stars and Tc-poor S stars. These families have orbital parameters similar to those of symbiotic systems but do not exhibit symbiotic activity. The hot component of most symbiotic systems is a white dwarf and, at least in some systems, the white dwarf mass is higher than 0.5 $M_\odot$ (Mikołajewska 2003). White dwarfs of this type have gone through the TP-AGB phase. Moreover, the orbital periods of the S-symbiotic systems are generally less than ~1000 days with circular orbits. Interaction of these systems is via Roche-lobe overflow. Jorissen (2003) suggested that either the former AGB star did not go through the TP-AGB or its high metallicity hindered the efficiency of the s-process and the mass transfer during the TP-AGB. The first possibility could apply to a small number of red symbiotic systems with low mass ($M_{\rm WD}$ ~0.4 $M_\odot$) companions such as AX Per and CI Cyg. However, in order to account for the absence of the barium syndrome in systems like AR Pav ($M_{\rm WD}$ ~1 $M_\odot$) or FN Sgr ($M_{\rm WD}$ ~0.7 $M_\odot$) the second possibility must be invoked.

There are contradictory arguments provided by the photospheric abundance analysis of symbiotic giants. In particular, the so-called yellow symbiotic systems, AG Dra, BD-21 3873, and He2-467, all contain K-type giants that are metal poor and s-process over abundant (Smith et al. 1996, 1997; Pereira et al. 1998). These systems seem to belong to the Galactic halo and are probably low-metallicity relatives of Ba stars. On the other hand, HD 330036, AS 201, and StHA 190, members of another small subclass of symbiotic stars with G-type giants and warm dust shells (D'-type), have very high rotational velocities, solar metallicities, and are also s-process over abundant (Smith et al. 2001, Pereira et al. 2005).

The vast majority of symbiotic systems, however, seem to contain normal M-type giants with very little known about their abundances and no published information about the presence of any s-process enrichments (Schmidt et al. 2006, and references therein). Thus far most information about the red giant nature and chemistry is derived either from the abundance studies based on nebular emission lines (Nussbaumer et al. 1988) or (mostly) TiO molecular absorption bands (Mürset & Schmid 1999). In addition, analysis of the first-overtone CO absorption features in *K*-band spectra of a dozen symbiotic systems indicate sub-solar carbon abundances and $^{12}C/^{13}C$ ~ 3 to 30 (Schild et al. 1992, Schmidt & Mikołajewska 2003, Schmidt et al. 2006). All these have indicated that the surveyed symbiotic giants are indistinguishable from local M giants in agreement with abundance studies based on nebular emission lines.

Despite the significant role that knowledge of chemical composition has to play in improving our understanding of the symbiotic systems, there are few cases in which abundances are fairly well determined. Analysis of photospheric chemical abundances has been performed only for a few bright systems: CH Cyg - the brightest symbiotic system (Schmidt et al. 2006), V2116 Oph - the symbiotic system with a neutron star (Hinkle et al. 2006), and the symbiotic recurrent novae T CrB and RS Oph (Wallerstein et al. 2008). In all these cases a solar or nearly solar metallicity was found with Li enhancements in RS Oph and T CrB the only peculiarity. For CH Cyg Schmidt et al. (2006) found that the isotopic ratios of $^{12}C/^{13}C$ and $^{16}O/^{17}O$ are close to the mean values for single M giants that have experienced the first dredge-up. The relatively high metallicity of CH Cyg accounts for the absence of chemical peculiarities similar to those seen in Ba stars. The analysis of Schmidt et al. (2006) has also revealed significant differences between the C/N and O/N ratios derived from nebular emission lines versus those from photospheric absorption lines. This indicates that an analysis based on emission lines can, for some circumstances, seriously overestimate the N abundance. A direct high resolution spectroscopic determination of the photospheric chemical abundances of red symbiotic giants is needed to settle this issue and to explore the abundances of more members of the symbiotic family.

We have undertaken an extensive research program to perform detailed chemical composition analysis of a sample of over 30 symbiotic systems. The analysis is based on near-*IR* spectra observed at high-resolution (R ~ 50000) and high S/N (~100) during the years 2003-2006 with the Phoenix spectrometer on the Gemini South telescope. The spectral regions observed are located in the *H* and *K* photometric bands. Spectrum synthesis employing standard LTE analysis and current model atmospheres was used to determine abundances of CNO and elements around the iron peak (Sc, Ti, Fe, and Ni) in the stellar photospheres. We expect our study to provide clues to resolve the metallicity problem in symbiotic systems as well as important information for understanding the history of these systems.

In this paper we present the first analysis of the photospheric chemical abundances (CNO and elements around iron peak: Sc, Ti,

Table 3. Velocity parameters [a] of the cool components obtained via cross-correlation technique

	RW Hya		
	$(V_{\rm rot}^2 \sin^2 i + \xi_{\rm t}^2)^{0.5}$	$V_{\rm rad}$	Orbital phase
Feb 2003	5.74	11.13 ± 0.15	0.57
Apr 2003	6.63	3.04 ± 0.34	0.74
Dec 2003	6.25	18.44 ± 0.32	0.38
Apr 2006	5.57	5.33 ± 0.41	0.65
	SY Mus		
	$(V_{\rm rot}^2 \sin^2 i + \xi_{\rm t}^2)^{0.5}$	$V_{\rm rad}$	Orbital phase
Feb 2003	3.88	19.39 ± 0.15	0.02
Apr 2003	5.98	19.66 ± 0.29	0.12
Dec 2003	6.84	13.14 ± 0.41	0.50
Apr 2006	5.01	4.42 ± 0.37	0.84

[a] Units km s^{-1}

Table 4. Quadrature sums of the projected rotational velocities and micro-turbulence $(V_{\rm rot}^2 \sin^2 i + \xi_{\rm t}^2)^{0.5}$ from *K*-band Ti I, Fe I and Sc I lines [a]

	RW Hya	SY Mus
Apr 2003	6.73 ± 0.60	6.91 ± 0.33
Dec 2003	6.35 ± 0.24	6.97 ± 0.33
both [b]	6.54 ± 0.32	6.94 ± 0.22

[a] Units km s^{-1}

[b] Used for synthetic spectra calculations

Fe, and Ni) for two classical S-type symbiotic systems, RW Hya and SY Mus. Both of these systems have well known basic parameters (Table 1) with effective temperatures estimated from the near-IR colors. Both systems also have well established orbital solutions with circular orbits. Near-IR light curves of both systems show ellipsoidal variations which permit an estimation of their red giant radii (Rutkowski et al. 2007). These two systems have tidally distorted giants similar to those in the classical Z And-type symbiotic systems but unlike these systems they do not show outburst activity.

2 OBSERVATIONS AND DATA REDUCTION

Spectra of RW Hya and SY Mus were observed at high-resolution ($R = \lambda/\Delta\lambda \sim 50000$) and high S/N ratio ($\gtrsim 100$) in the near-IR using the Phoenix cryogenic echelle spectrometer on 8 m Gemini South telescope. For both objects one spectrum was observed at 1.56 μm (*H*-band) during February 2003, two spectra at 2.23 μm (*K*-band) during April and December 2003, and one spectrum at 2.36 μm ($K_{\rm r}$-band) during April 2006. All the spectra cover a narrow spectral range of ∼100Å. The spectra were extracted and wavelength calibrated using standard reduction techniques (Joyce 1992) and all were heliocentric corrected. In all cases telluric lines were either not present in the interval observed or were removed by reference to a hot standard star. For all spectra the Gaussian instrumental profile is about of 6 km s^{-1} FWHM, corresponding to instrumental profile widths of 0.31 Å , 0.44 Å and 0.47 Å for the *H*-band, *K*-band, and $K_{\rm r}$-band spectra, respectively. The journal of our spectroscopic observations is given in Table 2 and the spectra of RW Hya and SY Mus are shown in Figures 1–3 and 4–6, respectively.

Table 5. Calculated abundances and relative abundances [a], velocity parameters [b], and uncertainties [c] for RW Hya and SY Mus

	RW Hya		SY Mus		
X	$\log \epsilon(X)$	$[X]$	$\log \epsilon(X)$	$[X]$	n [d]
^{12}C	7.53±0.02	-0.90±0.07	8.17±0.01	-0.26±0.06	90
N	7.46±0.03	-0.37±0.08	8.11±0.02	+0.28±0.07	62
O	8.17±0.01	-0.52±0.06	8.66±0.01	-0.03±0.06	49
Sc	2.71±0.05	-0.44±0.09	3.97±0.05	+0.82±0.09	1
Ti	4.49±0.05	-0.46±0.10	5.12±0.03	+0.17±0.08	9
Fe	6.74±0.02	-0.76±0.06	7.42±0.02	-0.08±0.06	21
Ni	5.63±0.03	-0.59±0.07	6.37±0.03	+0.15±0.07	3
^{12}C/^{13}C	6±2	...	10±3	...	$\frac{66}{16}$ [e]
$\xi_{\rm t}$	1.8±0.2		2.0±0.2		...
$V_{\rm rot} \sin i$	6.3±0.2		6.6±0.2		...

[a] Relative to the Sun $[X]$ abundances estimated in relation to the solar composition of Asplund et al. (2009)

[b] Units km s^{-1}

[c] 3σ

[d] Number of lines used

[e] Number of lines used to estimate ^{12}C/^{13}C isotopic ratio: 66 lines for ^{12}C and 16 lines for ^{13}C.

3 ANALYSIS AND RESULTS

The observed *H*-band region is dominated by strong molecular lines from the CO second overtone, OH first overtone, and relatively weak CN red systems lines. It also contains numerous atomic absorption lines mainly from Fe I with a few Ti I and Ni I lines. The *K*-band region is dominated by atomic Ti I, Fe I, and Sc I lines. There are also numerous weak CN molecular lines. Ca I and Ba I atomic lines are also present but too weak to be useful in chemical abundance analysis. $K_{\rm r}$-band region has strong first overtone CO molecular absorption lines coming from transitions quite far from the band head. This results in slight problems in reliably setting the continuum. While dominated by lines from ^{12}CO the presence of lines from the ^{13}CO isotopologue (mainly from the 2–0 transition) make this spectrum useful for evaluating the ^{12}C/^{13}C isotopic ratio. There are also three atomic lines, two from Fe I and one from Sc I.

The analysis was performed by fitting synthetic spectra to the observed spectra using a similar method to that used by Schmidt et al. (2006) in evaluating the CH Cyg abundances. The calculations of synthetic spectra over the entire observed spectral region were performed using the code WIDMO developed by M.R. Schmidt (Schmidt et al. 2006). To perform the χ^2 minimization a special overlay was performed on the code WIDMO with use of the simplex algorithm. This procedure used the method described in Brandt (1998) and the flowchart of Kallrath & Milone (1999). To evaluate quantitatively the fit quality, the residuals were calculated during each iteration, by differencing the synthesized and observed spectra at each point in the used spectral range. The simplex algorithm searched for the minimum of the standard deviation of the residuals to find an optimal fit.

For elemental abundance determination stellar effective temperature ($T_{\rm eff}$) and surface gravity ($\log g$) are required as input parameters. In addition information about micro- and macro-turbulences, line identifications with values of quantities that characterize the transitions and the models of the atmospheres are needed. MARCS model atmospheres developped by Gustafsson et al. (2008) were used in our calculations. The input effective temperatures ($T_{\rm eff}$) were estimated from the known spectral

Table 6. Calculated abundances and relative abundances [a] for RW Hya and SY Mus where all radial and rotational parameters were set as a free parameters

	RW Hya		SY Mus		
X	$\log\epsilon(X)$	$[X]$	$\log\epsilon(X)$	$[X]$	n [b]
^{12}C	7.54	-0.89	8.10	-0.33	90
N	7.46	-0.37	8.11	+0.28	62
O	8.17	-0.52	8.58	-0.11	49
Sc	2.75	-0.40	4.02	+0.87	1
Ti	4.54	-0.41	5.13	+0.18	9
Fe	6.75	-0.75	7.39	-0.11	21
Ni	5.63	-0.59	6.36	+0.14	3
^{12}C/^{13}C	5.0	...	8.0	...	$\frac{66}{16}^{\star}$

[a] Relative to the Sun $[X]$ abundances estimated in relation to the solar composition of Asplund et al. (2009)

[b] Number of lines used, ^{12}C/^{13}C number as in Table 5

Table 7. Velocity parameters [a] of the cool giants where radial and rotational parameters were set as a free parameters

	RW Hya		
ξ_t	1.74 ± 0.27		
	$V_{rot}\sin i$	V_{rad}	Orbital phase
Feb 2003	6.0 ± 0.4	11.09 ± 0.47	0.57
Apr 2003	6.6 ± 0.7	2.85 ± 0.59	0.74
Dec 2003	7.1 ± 0.5	18.77 ± 0.31	0.38
Apr 2006	8.9 ± 0.5	5.06 ± 0.35	0.65
	SY Mus		
ξ_t	1.95 ± 0.30		
	$V_{rot}\sin i$	V_{rad}	Orbital phase
Feb 2003	5.4 ± 0.5	19.28 ± 0.26	0.02
Apr 2003	5.9 ± 0.6	19.77 ± 0.38	0.12
Dec 2003	6.6 ± 0.5	13.26 ± 0.36	0.50
— Apr 2006	6.5 ± 0.6	4.40 ± 0.20	0.84

[a] Units km s^{-1}

types, M2 and M5 (Belczyński et al. 2000, and references therein), adopting the calibration by Richichi et al. (1999). The resulting values are $T_{\rm eff}$ = 3655 ± 80 K for RW Hya and $T_{\rm eff}$ = 3355 ± 75 K for SY Mus. A $(J-K)$ color of 1.15 and 1.40 (Rutkowski et al. 2007) and color excesses $E(B-V)$ = 0.02–0.10 and 0.4–0.5 results in intrinsic colors of $(J-K)_0$ ∼1.1 and ∼1.2 for RW Hya and SY Mus. Using the Kucinskas et al. (2005) $T_{\rm eff}$–log g–color relation for late-type giants we can estimate the effective temperatures as 3600–3700 K and ≲3500 K, respectively, in good agreement with the above values. The surface gravities from this relation are $\log g \approx 0.5$ in both cases, in agreement with the values derived from the published red giant parameters (Table 1), $\log g \approx 0.5$ and $\log g \approx 0.3$ for RW Hya and SY Mus, respectively. As a result the model atmospheres used had $\log g = 0.5$, solar chemical composition ([Fe/H] = 0.0), and effective temperatures of $T_{\rm eff}$ = 3700 K and $T_{\rm eff}$ = 3400 K for RW Hya and SY Mus, respectively. In the case of RW Hya our analysis revealed significantly sub-solar metallicity, [Fe/H]∼-0.7. The whole analysis was therefore repeated adopting the model atmosphere with [Fe/H]=-0.75.

We used a number of standard sources to characterize the spectral lines. For the macroturbulence velocity, ζ_t, we used 3 km s^{-1}, typical for cool red giants (see for example Fekel et al. 2003). The atomic data were taken from the VALD database (Kupka et al. 1999) in the case of K- and K_r-bands and from the list given by Mélendez & Barbuy (1999) in the H-band. The vacuum wavelengths, excitation potentials, and gf-values for the vibration-rotation lines of CO isotopes are adopted from Goorvitch (1994). The lists of ^{12}CN, and OH molecular lines were adopted from the database of Kurucz (1999). The complete list of the lines identified and selected for our abundance analysis, with the excitation potentials (EP) and gf-values for transitions, is shown in TablesA1 and A2 in the Appendix.

To fit synthetic spectra to observed spectra it is necessary to find, in addition to the parameters of chemical composition (C, N, O, Sc, Ti, Fe, Ni in this case), values for a number of velocities. These include the microturbulent velocity, ξ_t, the radial velocity, $V_{\rm rad}$, and the rotational velocity, $V_{\rm rot}\sin i$. The adopted strategy relies on handling the three spectral regions in the H- and K-band ranges as if they were a single spectrum to obtain a solution for the chemical composition. The chemical composition should not depend on the orbital phase. One set of the abundance parameters and microturbulent velocity will apply to all spectra of a given object. On the other hand, the radial velocities $V_{\rm rad}$ depend on the orbital phase and the rotational velocities $V_{\rm rot}\sin i$ can also depend on tidal forces in the outer regions of the giant.

To obtain radial and rotational velocities we used a cross-correlation technique similar to that of Carlberg et al. (2011). The method enables the evaluation of rotational velocities in spectra rich with lines where unblended lines are rare, as is the case of our H- and K_r-band spectra. For templates we used synthetic spectra generated from the line list of Appendix A (TablesA1 and A2) broadened only by the instrumental profile. We measured the FWHM of the cross-correlation peak, $\mu_\star$, for each observed spectrum and the FWHM of auto-correlation peak, μ_t, for each appropriate template using IRAF's *fxcor* task. The widths of spectral lines attributable to stellar processes were obtained by subtraction of the contributions from the template and instrumental profile, $\omega_\star = (\mu_\star^2 - 0.5\mu_t^2 - \omega_i^2)^{0.5}$. Next the quantity $\omega_\star$ was converted to a so called total stellar broadening ($\beta_{\rm Gray}$) using a second order polynomial applicable to FWHM measurements made at any wavelength in velocity units (eq. 1 in Carlberg et al. 2011): $\omega_\star({\rm kms}^{-1}) = 1.89582 + 1.16526\beta_{\rm Gray} + 0.0065\beta_{\rm Gray}^2$. Finally we obtained the quadrature sums of the projected rotational velocities and microturbulence: $(V_{\rm rot}^2\sin^2 i + \xi_t^2)^{0.5} = (\beta_{\rm Gray}^2 - \zeta_t^2)^{0.5}$. The velocity parameters derived are shown in Table3.

Our K-band spectra contain a few relatively strong atomic lines that are not blended. These lines enable a direct measurement of the FWHMs of the stellar line profiles. Fekel et al. (2003) used three Ti I, two Fe I, and one Sc I line to measure rotational velocities in a dozen symbiotic systems. We used the same lines to measure rotational velocities in RW Hya and SY Mus based on the total stellar broadening $\beta_{\rm Gray}$ for each spectrum separately and for 12 lines from both spectra simultaneously. To measure FWHMs the IRAFs *splot* tool have been used. The results are shown in Table 4. The values are in agreement within the uncertainties with those obtained via another method (see Tables 3 and 7).

To perform solutions using the simplex algorithm $n+1$, n dimensional sets of free parameters must be prepared that form a grid in parameter space called simplex (see e.g. Kallrath & Milone 1999; Brandt 1998). We have 7 free parameters for abundances. Two additional free parameters are the projected rotational velocity ($V_{\rm rot}\sin i$) and microturbulence (ξ_t). The quadrature sum of these quantities is treated as a constant adopted from the previously ob-

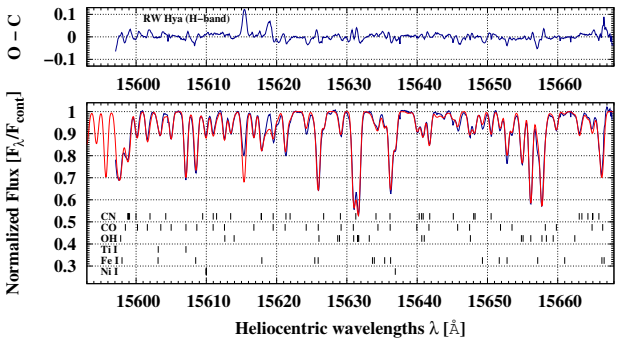

Figure 1. The spectrum of RW Hya observed in February 2003 (thin line) in the *H*-band and a synthetic spectrum (thick line) calculated using the final abundances and $^{12}C/^{13}C$ isotopic ratio (Table 5). Molecular (OH, CO, CN) and atomic (Ti I, Fe I, Ni I) lines used in the solution of the chemical composition are identified by ticks.

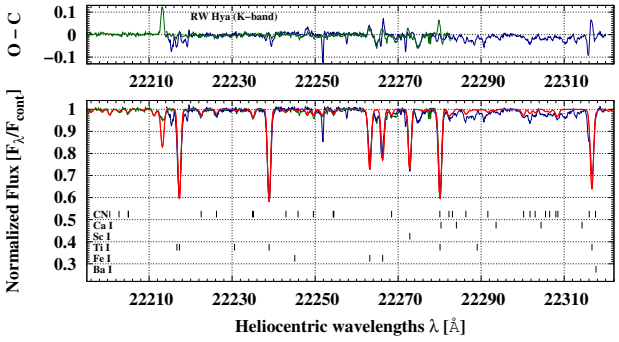

Figure 2. Spectra of RW Hya observed in April 2003 (thin solid line) and December 2003 (thin dot-dashed line) in the *K*-band and a synthetic spectrum (thick solid line) calculated using the final abundances and $^{12}C/^{13}C$ isotopic ratio (Table 5). Molecular (CN) and atomic (Sc I, Ti I, Fe I) lines used in the solution of the chemical composition are identified by ticks.

tained value (see Table 4). To estimate the input abundance parameters the adopted procedure was as follows. As a first approximation solar composition (Asplund et al. 2009) was adopted and the oxygen abundance was found by fitting (by eye) the OH lines in the *H*-band spectrum. The carbon abundance was adjusted next to find the best fit to the CO lines. Following this the nitrogen abundance was adjusted by fitting the CN lines in *H*- and *K*-band spectra. The last step was to fit the atomic lines. The procedure was repeated for several iterations. In this way the initial values of the free parameters were found around which the simplexes were build.

Nine different initial simplexes were used in both the RW Hya and SY Mus cases with each repeated with different values of the microturbulent velocity ξ_t. Although the microturbulent velocity is a free parameter in our solution it is not an element of the simplex. Rather the best value was searched for in the 1.2–2.6 km s^{-1} range with use of golden ratio method. After we found the sets of parameters that give the best fit to *H*- and *K*-band spectra we applied the derived chemical abundances to the K_r spectrum as a fixed parameter and we searched for the $^{12}C/^{13}C$ ratio with the rotational velocity as an additional free parameter. After obtaining the optimal fit we made a reconciliation of ^{12}C abundance and $^{12}C/^{13}C$ isotopic ratio within 3 iterations. The final abundances for CNO elements and atomic lines (Sc I, Ti I, Fe I, Ni I) in the scale of $\log \epsilon(X) = \log N(X)N(H)^{-1} + 12.0$, the isotopic ratios $^{12}C/^{13}C$, microturbulences and projected rotational velocities are summarized in Table 5 together with the formal uncertainties. Our final synthetic spectra fitted to the observed ones are show in Figures 1–6. Additionally, we obtained independent solutions for each spectrum for the case when all radial and rotational velocities are treated as a free parameters. The resulting abundances are shown in Table6 and the velocity parameters are shown in Table 7, and the final synthetic spectra fitted to the observed ones are presented in Figures 7–10.

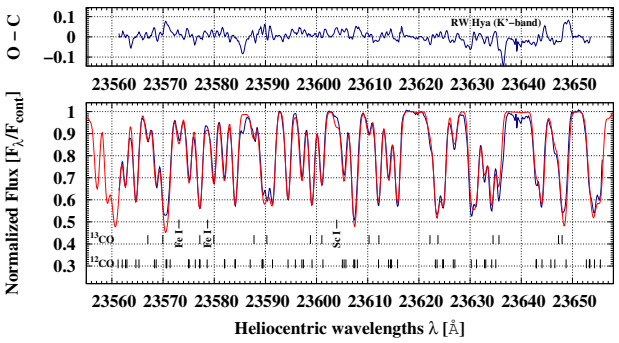

Figure 3. The spectrum of RW Hya observed in April 2006 (thin line) in the K_r-band and a synthetic spectrum (thick line) calculated using the final abundances and $^{12}C/^{13}C$ isotopic ratio (Table 5). Molecular (^{12}CO, ^{13}CO) and atomic (Sc I, Fe I) lines are identified by ticks.

We also made additional fits with MARCS atmosphere models varying the effective temperatures by ±100 K, and $\log g$ and the microturbulence, ξ_t, by ±0.5, and in, the case of RW Hya, also the metallicity [Fe/H] by +0.25 to estimate the sensitivity of abundances to uncertainties in stellar parameters: T_{eff}, $\log g$, ξ_t, for each species. The changes in the abundance for each element as a function of each stellar parameter are listed in Tables 8. Uncertainties in the stellar parameters have the strongest impact on the accuracy of the obtained chemical composition.

The abundance of scandium is based only on one strong Sc I line at $\lambda \sim 22272.8$Å and it may be less reliable than other abundances. There are two another scandium Sc I lines present in *K*-band spectrum at $\lambda \sim 22213.2$Å and $\lambda \sim 22208.7$Å (see Appendix TableA1). However they show quite different behaviour and when used they indicate an abundance lower by ∼1 dex. We suspect, the atomic data published for these transitions are not reliable. The use of other published data for these transitions (eg. Pehlivan (2012) or Wiese & Fuhr (1975)) leads to almost identical results. Broadening of the infrared Sc I lines by hyperfine structure (Aboussaid et al. 2006) has not been included in the analysis.

4 DISCUSSION

To fit the synthetic spectra it is necessary to take into account the stellar motions (both the radial and rotational velocities) and also velocity fields below the stellar photosphere (turbulences). In section 3 we obtained the rotational and radial velocities via various methods (compare Tables 3, 4, and 7) as well as microturbulences (Tables 5 and 7). The microturbulent velocities ξ_t obtained in our solutions are self-consistent and are consistent with those obtained for Galactic M-type Giants by (Smith & Lambert 1990, 1990) and for LMC red giants by Smith et al. (2002).

The radial velocities we measured by cross-correlation and fitting synthetic spectra are perfectly compatible. The values obtained for RW Hya are in accord with synthetic radial velocities predicted

Table 8. Sensitivity of abundances to uncertainties in the stellar parameters

ΔX	$\Delta T_{\rm eff}$ = +100 K		$\Delta \log g$ = +0.5		$\Delta\xi_{\rm t}$ = +0.5		$\Delta[Fe/H]$ = +0.25
	RW Hya	SY Mus	RW Hya	SY Mus	RW Hya	SY Mus	RW Hya
C	+0.04	+0.03	+0.21	+0.22	-0.01	-0.07	0.03
N	+0.08	+0.04	-0.05	+0.02	-0.08	-0.12	0.16
O	+0.16	+0.12	+0.03	+0.08	-0.06	-0.10	0.14
Sc	+0.15	+0.12	+0.08	+0.15	-0.15	-0.61	0.03
Ti	+0.12	+0.08	+0.12	+0.15	-0.40	-0.50	0.07
Fe	-0.01	-0.04	+0.11	+0.15	-0.14	-0.15	0.02
Ni	-0.00	-0.04	+0.11	+0.21	-0.08	-0.23	0.01

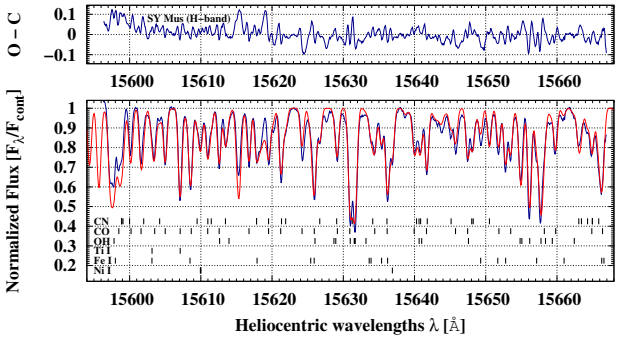

Figure 4. The spectrum of SY Mus observed in February 2003 in the *H*-band (thin line) and a synthetic spectrum (thick line) calculated using the final abundances and $^{12}C/^{13}C$ isotopic ratio (Table 5). Molecular (OH, CO, CN) and atomic (Ti I, Fe I, Ni I) lines used in the solution of the chemical composition are identified by ticks.

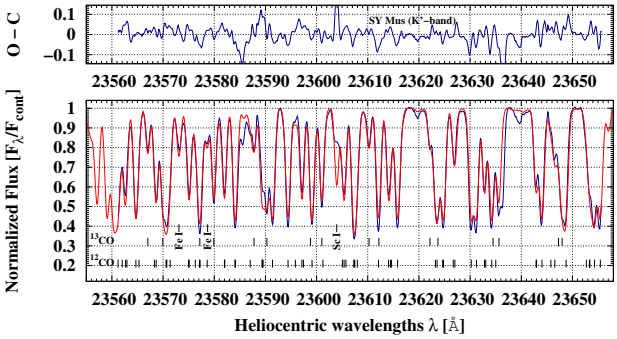

Figure 6. The spectrum of SY Mus observed in April 2006 (thin line) in the $K_{\rm r}$-band and a synthetic spectrum (thick line) calculated using the final abundances and $^{12}C/^{13}C$ isotopic ratio and $^{12}C/^{13}C$ isotopic ratio (Table 5). Molecular (^{12}CO, ^{13}CO) and atomic (Sc I, Fe I) lines are identified by ticks.

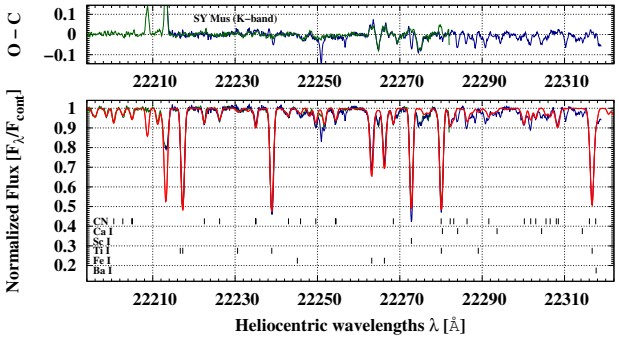

Figure 5. Spectra of SY Mus observed in April 2003 (thin solid line) and December 2003 (thin dot-dashed line) in the *K*-band and a synthetic spectrum (thick solid line) calculated using the final abundances and $^{12}C/^{13}C$ isotopic ratio (Table 5). Molecular (CN) and atomic (Sc I, Ti I, Fe I) lines used in the solution of the chemical composition are identified by ticks.

from the orbit of Kenyon & Mikołajewska (1995) with an accuracy generally better than 1 km s^{-1}. One spectrum observed on Feb 2003 is in poorer agreement, ~2 km s^{-1}. The radial velocities for SY Mus agree with synthetic velocities from the orbit of Dumm et al. (1998) with accuracy of ~ 1–2 km s^{-1}. The exception here is for a spectrum observed on Feb 2003 where the difference is large, ~5 km s^{-1}.

In these stars the rotational velocities, $V_{\rm rot} \sin i$, give the largest contribution to the physical line broadening. In the case of spectra with relatively strong atomic lines and weak molecular lines, like those in *K*-band region, the rotational velocity obtained by cross-correlation, by fitting synthetic spectra, and from FWHM of strong unblended lines give perfectly consistent results. However, velocities obtained for spectra with strong molecular lines (strongly blended) are considerably different depending on the method used and appear to be significantly underestimated by the cross-correlation method.

Our results obtained from the spectra taken at different, random orbital phases, differ slightly. The origin of these differences is not clear. On the one hand, if these stars were significantly tidally distorted, the projected rotational velocities might vary with orbital phase. On the other hand this could be due to strong blending of the lines in some spectra (discussed above) or maybe to the use of an uncertain value for the instrumental profile. However, in general these differences are only slightly higher than the limits set by the uncertainties. The only exception is somewhat higher rotational velocity derived for RW Hya from spectrum obtained in Apr 2006 than those resulting from the 2003 data. Fekel et al. (2003) estimated $V_{\rm rot} \sin i = 5 \pm 1$ km s^{-1} for RW Hya, measured in the *K*-band region, which is somewhat lower than our values.

Our analysis of the chemical abundances has revealed an approximately solar metallicity ([Fe/H]~0.0) for SY Mus and significantly sub-solar metallicity ([Fe/H]~-0.75) for RW Hya. CNO abundances in SY Mus (Tables 5 and 6) are close to the averaged values for 'normal' single M giants obtained by Smith & Lambert (1990). In RW Hya the CNO abundances are significantly reduced.

Cunha & Smith (2006) showed that different stellar populations are separated in the [O/Fe]-[Fe/H] plane. Figure 11 shows the position of RW Hya, and SY Mus in Fig. 5 of Cunha & Smith (2006). The symbiotic star CH Cyg is also plotted with its abundances derived by Schmidt et al. (2006). The values of [O/Fe] ver-

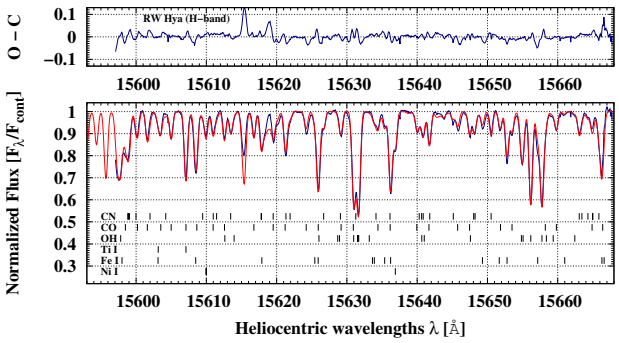

Figure 7. The spectrum of RW Hya observed in February 2003 in the *H*-band (thin line) and a synthetic spectrum (thick line) calculated using the final abundances and $^{12}C/^{13}C$ isotopic ratio (Table 6). This is the case where all radial and rotational parameters were allowed to be free parameters for the solution. Molecular (OH, CO, CN) and atomic (Ti I, Fe I, Ni I) lines used in the solution of the chemical composition are identified by ticks.

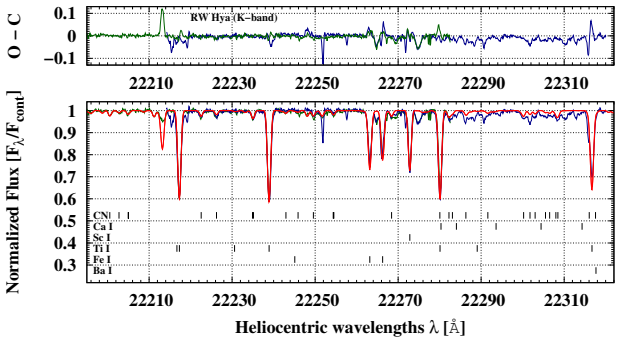

Figure 8. Spectra of RW Hya observed in April 2003 (thin solid line) and December 2003 (thin dot-dashed line) in the *K*-band and a synthetic spectrum (solid line) calculated using the final abundances and $^{12}C/^{13}C$ isotopic ratio (Table 6). This is the case where all radial and rotational were allowed to be free parameters for the solution. Molecular (CN) and atomic (Sc I, Ti I, Fe I) lines used in the solution of the chemical composition are identified by ticks.

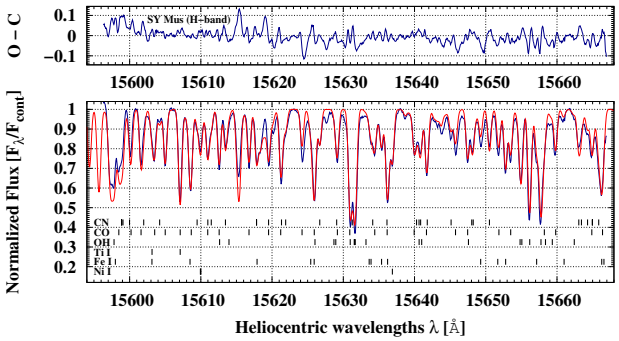

Figure 9. The spectrum of SY Mus observed in February 2003 in the *H*-band (thin line) and a synthetic spectrum (thick line) calculated using the final abundances and $^{12}C/^{13}C$ isotopic ratio (Table 6). This is the case where all radial and rotational parameters were allowed to be free parameters for the solution. Molecular (OH, CO, CN) and atomic (Ti I, Fe I, Ni I) lines used in the solution of the chemical composition are identified by ticks.

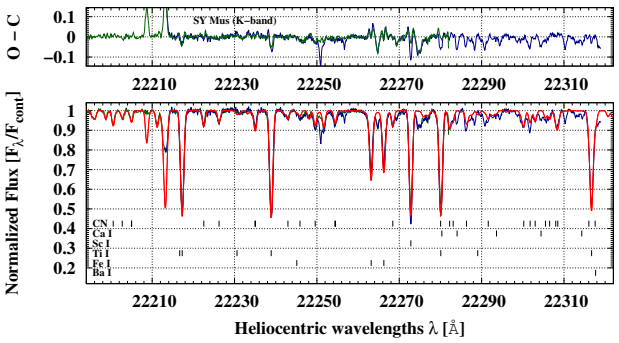

Figure 10. Spectra of SY Mus observed in April 2003 (thin solid line) and December 2003 (thin dot-dashed line) in the *K*-band and a synthetic spectrum (solid line) calculated using the final abundances and $^{12}C/^{13}C$ isotopic ratio (Table 6). This is the case where all radial and rotational parameters were allowed to be free parameters for the solution. Molecular (CN) and atomic (Sc I, Ti I, Fe I) lines used in the solution of the chemical composition are identified by ticks.

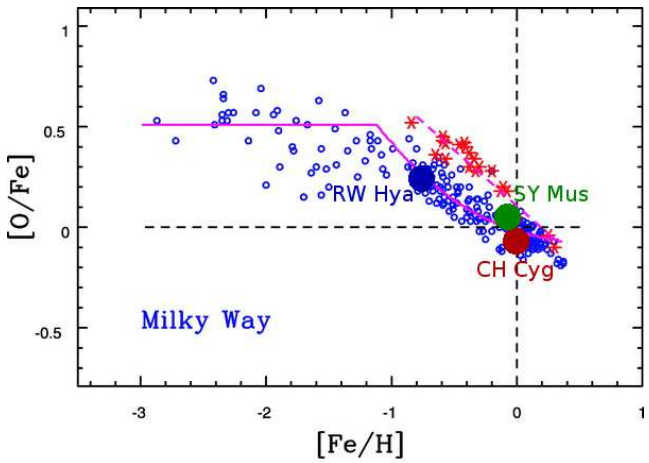

Figure 11. Oxygen relative to iron for various stellar populations (Cunha & Smith 2006). The position of RW Hya indicates membership in the thick disc/halo whereas SY Mus and CH Cyg are members of the thin disc.

sus [Fe/H] for RW Hya locate it among the thick disk/halo giants whereas those of SY Mus, and CH Cyg are typical for thin disk objects. These results are consistent with the location of these objects in the Milky Way, as well as their systemic velocities and proper motions. In particular, RW Hya has a relatively high galactic latitude, $b = 36.5°$, and appreciable proper motion, $\mu_\alpha \cos\delta = -18.6 \pm 1.6$ mas and $\mu_\delta = 14.1 \pm 1.6$ mas (Hog et al. 2003). Its significant proper motion has been known for a long time which led Tifft & Greenstein (1958) to suggestion that RW Hya is a halo object. The sub-solar metallicity derived for RW Hya is quite remarkable as it may host a relatively massive, ~0.8 $M_\odot$, white dwarf (Otulakowska-Hypka et al. 2013) and the present giant could be polluted by s-process elements from the former TP-AGB companion. Unfortunately, our infrared spectra do not cover any s-process element lines.

According to the predictions of the stellar evolution models the abundance of the ^{13}C isotope in the photospheres of low mass stars should increase due to extensive mixing processes during the ascent of the red giant branch (RGB). The very low $^{12}C/^{13}C$ iso-

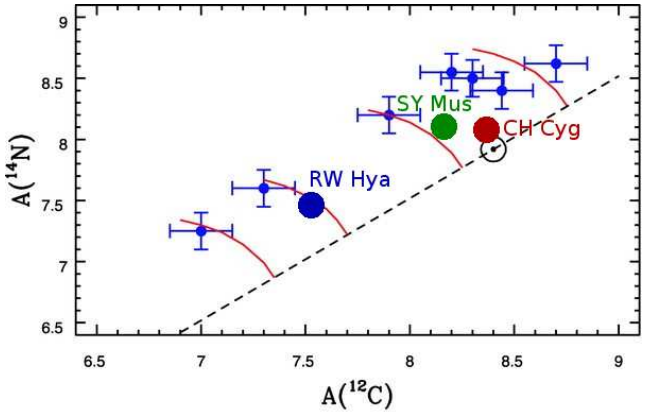

Figure 12. Nitrogen relative carbon for the stars from Cunha & Smith (2006) and our targets. The dashed line represents scaled solar abundances, [^{12}C/Fe]=0 and [^{14}N/Fe]=0, whereas the solid curves delineate constant ^{12}C+^{13}C 'CN mixing lines'.

topic ratios obtained for RW Hya and SY Mus (Tables 5 and 6) indicate that their giants have experienced first dredge-up when they were enriched in the ^{13}C isotope and that they belong to a population with medium or low metallicity (see Keller et al. 2001). Cunha & Smith (2006) adapted C and N abundances for monitoring the dredge-up on the RGB in the Galactic bulge. In Figure 12 ^{12}C and ^{14}N abundances are plotted for RW Hya and SY Mus as well as those for CH Cyg from Schmidt et al. (2006, Fig. 4). The location of RW Hya, and SY Mus overlap with the bulge red giants in the ^{14}N-rich region whereas CH Cyg remains near the solar line. The conclusion from of this plot is that the CN mixing has been more extensive in RW Hya and SY Mus than in CH Cyg. This is also reflected in the lower isotopic ratios, ^{12}C/^{13}C=6 and 8, in the former two objects as compared with ^{12}C/^{13}C=18 in CH Cyg (Schmidt et al. 2006).

5 CONCLUSIONS

We have performed a detailed analysis of the photospheric abundances of CNO and elements around the iron peak (Sc, Ti, Fe, and Ni) for the red giant components of RW Hya and SY Mus. Our analysis reveals a significantly sub-solar metallicity ([Fe/H]~-0.75) for the RW Hya giant, confirming its membership in the Galactic halo population, and a near-solar metallicity in SY Mus. The very low ^{12}C/^{13}C isotopic ratios, ~6–10, derived for both objects and their N enrichment indicate that the giants have experienced the first dredge-up.

6 ACKNOWLEDGMENTS

This study is supported by the Polish National Science Centre grant DEC-2011/01/B/ST9/06145. The observations were obtained at the Gemini Observatory, which is operated by the Association of Universities for Research in Astronomy, Inc., under a cooperative agreement with the NSF on behalf of the Gemini partnership: the National Science Foundation (United States), the National Research Council (Canada), CONICYT (Chile), the Australian Research Council (Australia), Ministério da Ciência, Tecnologia e Inovação (Brazil) and Ministerio de Ciencia, Tecnología e Innovación Productiva (Argentina). K.H. acknowledges travel support from the NOAO Office of Science. M.G. has been financed by the GEMINI-CONICYT Fund, allocated to the project 32110014.

REFERENCES

Aboussaid, A., Carleer, M., Hurtmans, D., Biémont, E., & Godefroid, M.R. 2006, Physica Scripta, 53, 28
Asplund, M., Grevesse, N., Sauval A., & Scott, P., 2009, ARAA 47, 481
Belczyński, K., Mikołajewska, J., Munari, U., et al., 2000, A&AS, 146, 407
Brandt, S., Data Analysis, Statistical and Computational Methods, 1998, Polish edition (Polish Scientific Publishers PWN)
Carlberg, J. K., Majewski, S. R., Patterson, R. J., et al., 2011, ApJ, 732, 39
Cunha, K., & Smith, V. V., 2006, ApJ, 651, 491
Davidsen, A., Malina, R., Bowyer, S., 1977, ApJ, 211, 866
Dumm, T., Schmutz, W., Schild, H., Nussbaumer, H., 1999, A&A, 349, 169
Fekel, F. C., Hinkle, H. K., Joyce, R. R., et al., 2003, ASPC, 303, 113
Garcia, M., Baliunas, S. L., Elvis, M., et al., 1983, ApJ, 267, 291
Goorvitch, D., 1994, ApJS, 95, 535
Gustafsson, B., Edvardsson, B., Eriksson, K., et al., 2008, A&A, 486, 951
Hinkle, K. H., Fekel, F. C., Joyce, R. R., et al., 2006, ApJ, 641, 479
Hog, E., Fabricius, C., Makarov, et al., 2000, A&A, 355, L27
Jorissen, A., 2003, ASPC, 303, 25
Joyce, R. 1992, in ASP Conf. Ser. 23, Astronomical CCD Observing and Reduction Techniques, ed. S. Howell (San Francisco: ASP), 258
Kallrath, J., & Milone, E. F., Eclipsing binary stars modeling and analysis, 1999, (New York: Springer)
Keller, L. D., Pilachowski, C. A., Sneden, C., 2001, AJ, 122, 2554
Kenyon, S. J., & Mikołajewska, J., 1995, AJ, 110, 391
Kucinskas, A., Hauschildt, P. H., Ludwig, H.-G., et al., 2005, A&A, 442, 281
Kupka, F., Piskunov, N., Ryabchikova, T., et al., 1999, A&AS, 138, 119
Kurucz, R. L., 1999, *http://kurucz.harvard.edu*
Mélendez, J., & Barbuy, B., 1999, ApJS, 124, 527
Mikołajewska, J. 2003, in "Symbiotic Stars Probing Stellar Evolution", ASP Conference Proceedings, eds. R. L. M. Corradi, J. Mikołajewska and T. Mahoney, 303, p.9.
Mürset, U., & Schmid, H. M., 1999, A&AS, 137, 473
Nussbaumer, H., Schild, H., Schmid, H. M., Vogel, M., 1988, A&A, 198, 179
Otulakowska-Hypka, M., Mikołajewska, J., Whitelock, P., 2013, in *Stella Novae: Future and Past Decades*, ASPC, in press
Pehlivan Asli, 2012, "Laboratory Spectroscopy of Neutral Scandium, ScÍ, for Astrophysical Application" MSc thesis at Lund Observatory
Pereira, C. B., Smith, V. V., Cunha, K., 1998, AJ, 116, 1977
Pereira, C. B., Smith, V. V., Cunha, K., 2005, A&A, 429, 993
Richichi, A., Fabbroni, L., Ragland, S., Scholz, M., 1999, A&A, 344, 511
Rutkowski, A., Mikołajewska, J., & Whitelock, P., 2007, Baltic Astronomy, 16, 49
Schild, H., Murset, U., & Schmutz, W., 1996, A&A, 306, 477
Schild, H., Boyle, S. J., Schmid, H. M., 1992, MNRAS, 258, 95

Schmidt, M. R., & Mikołajewska, J., 2003, ASPC, 303, 163
Schmidt, M. R., Zacs, L., Mikołajewska, J., & Hinkle, K., 2006, A&A, 446, 603
Schmutz, W., Schild, H., Murset, U., & Schmid, H., 1994, ApJ, 556, 55
Smith, V. V., & Lambert, D., 1986, ApJ, 311, 843
Smith, V. V., & Lambert, D., 1990, ApJS, 72, 387
Smith, V. V., Cunha, K., Jorissen, A., Boffin, H. M. J., 1996, A&A, 315, 179
Smith, V. V., Cunha, K., Jorissen, A., Boffin, H. M. J., 1997, A&A, 324, 97
Smith, V. V., Pereira, C. B., Cunha, K., 2001, ApJ, 556, 55
Smith, V. V., Hinkle, K. H., Cunha, K., 2002, AJ, 124, 3241
Tifft, W. G., & Greenstein, J. L., 1958, ApJ, 127, 160
Wallerstein, G., Harrison, T., Munari, U., Vanture, A., 2008, PASP, 120, 492
Wiese, W. L., & Fuhr, J. R., 1975, J. Phys. Chem. Ref. Data, 4, 263

APPENDIX A: LIST OF ATOMIC AND MOLECULAR LINES

This paper has been typeset from a TEX/ LATEX file prepared by the author.

Table A1. List of atomic lines selected for calculations together with gf-values and excitation potentials.

Wavelength (air) [Å]	EP [eV]	$\log gf$	Ref.
Sc I			
‡22202.640	1.428	-3.436	Kupka et al. (1999)
‡22207.128	1.428	-1.836	Kupka et al. (1999)
22266.729	1.428	-1.327	Kupka et al. (1999)
‡ 23603.945	1.428	-2.180	Kupka et al. (1999)
Ti I			
15598.890	4.690	-0.030	Mélendez & Barbuy (1999)
15602.840	2.270	-1.810	Mélendez & Barbuy (1999)
22210.636	4.213	-1.444	Kupka et al. (1999)
22211.228	1.734	-1.770	Kupka et al. (1999)
22224.530	4.933	-0.263	Kupka et al. (1999)
22232.838	1.739	-1.658	Kupka et al. (1999)
22274.012	1.749	-1.756	Kupka et al. (1999)
22282.973	4.690	-0.586	Kupka et al. (1999)
22310.617	1.734	-2.124	Kupka et al. (1999)
Fe I			
15593.740	5.030	-1.980	Mélendez & Barbuy (1999)
15598.870	6.240	-0.920	Mélendez & Barbuy (1999)
15604.220	6.240	0.280	Mélendez & Barbuy (1999)
15613.630	6.350	-0.290	Mélendez & Barbuy (1999)
15621.160	6.200	-0.990	Mélendez & Barbuy (1999)
15621.650	5.540	+0.170	Mélendez & Barbuy (1999)
15629.370	5.950	-1.670	Mélendez & Barbuy (1999)
15629.630	4.560	-3.130	Mélendez & Barbuy (1999)
15631.110	3.640	-3.980	Mélendez & Barbuy (1999)
15631.950	5.350	-0.150	Mélendez & Barbuy (1999)
15645.010	6.310	-0.540	Mélendez & Barbuy (1999)
15647.410	6.330	-1.090	Mélendez & Barbuy (1999)
15648.520	5.430	-0.800	Mélendez & Barbuy (1999)
15652.870	6.250	-0.190	Mélendez & Barbuy (1999)
15656.640	5.870	-1.900	Mélendez & Barbuy (1999)
15662.010	5.830	+0.000	Mélendez & Barbuy (1999)
15662.320	6.330	-1.020	Mélendez & Barbuy (1999)
15665.240	5.980	-0.600	Mélendez & Barbuy (1999)
22239.040	5.385	-3.121	Kupka et al. (1999)
22257.097	5.064	-0.723	Kupka et al. (1999)
22260.185	5.086	-0.952	Kupka et al. (1999)
‡23566.671	6.144	0.306	Kupka et al. (1999)
‡23572.267	5.874	-0.886	Kupka et al. (1999)
Ni I			
15605.6800	5.300	-0.590	Mélendez & Barbuy (1999)
15605.7500	5.300	-1.010	Mélendez & Barbuy (1999)
15632.6200	5.310	-0.130	Mélendez & Barbuy (1999)

‡ Not used for the chemical composition determination.

Table A2. List of molecular lines selected for calculations together with gf-values and excitation potentials.

Wavelength (air) [Å]	EP [eV]	$\log gf$	Ref.
$^{12}C^{14}N$			
15594.607	0.9162	-1.645	Kurucz (1999)
15594.610	1.1079	-1.240	Kurucz (1999)
15594.816	1.1770	-1.097	Kurucz (1999)
15595.729	0.9218	-2.106	Kurucz (1999)
15597.719	1.3900	-1.443	Kurucz (1999)
15599.961	1.2391	-1.807	Kurucz (1999)
15605.217	1.2601	-1.810	Kurucz (1999)
15606.718	0.9095	-2.116	Kurucz (1999)
15607.198	1.5181	-1.318	Kurucz (1999)
15609.198	0.9361	-1.479	Kurucz (1999)
15613.554	1.0521	-1.645	Kurucz (1999)
15613.557	1.1770	-1.090	Kurucz (1999)
15615.246	1.0359	-1.645	Kurucz (1999)
15617.057	1.1080	-1.231	Kurucz (1999)
15617.646	1.3900	-1.435	Kurucz (1999)
15622.431	0.9162	-1.637	Kurucz (1999)
15624.806	1.5182	-1.311	Kurucz (1999)
15626.993	0.9345	-2.088	Kurucz (1999)
15629.867	1.2602	-1.798	Kurucz (1999)
15631.866	0.9362	-1.473	Kurucz (1999)
15636.015	0.9218	-2.097	Kurucz (1999)
15636.361	1.2816	-1.801	Kurucz (1999)
15636.584	1.1314	-1.231	Kurucz (1999)
15637.521	0.9357	-1.633	Kurucz (1999)
15640.865	1.4182	-1.436	Kurucz (1999)
15643.764	1.0688	-1.632	Kurucz (1999)
15643.965	1.0521	-1.632	Kurucz (1999)
15646.246	1.2059	-1.090	Kurucz (1999)
15658.785	1.1314	-1.223	Kurucz (1999)
15659.161	0.9476	-2.070	Kurucz (1999)
15660.014	1.5516	-1.313	Kurucz (1999)
15660.688	1.4182	-1.428	Kurucz (1999)
15660.705	1.2817	-1.789	Kurucz (1999)
15661.584	0.9612	-1.471	Kurucz (1999)
22194.477	1.2309	-1.747	Kurucz (1999)
22196.680	1.4573	-1.875	Kurucz (1999)
22198.914	1.4373	-1.872	Kurucz (1999)
22198.955	1.6007	-1.825	Kurucz (1999)
22216.477	1.2165	-1.747	Kurucz (1999)
22220.176	1.1036	-2.055	Kurucz (1999)
22228.924	1.1079	-2.204	Kurucz (1999)
22228.994	1.3036	-1.633	Kurucz (1999)
22236.898	1.1074	-2.249	Kurucz (1999)
22239.814	1.6007	-1.816	Kurucz (1999)
22243.514	1.2456	-1.732	Kurucz (1999)
22248.297	1.4573	-1.862	Kurucz (1999)
22248.438	1.4777	-1.866	Kurucz (1999)
22262.354	1.2309	-1.732	Kurucz (1999)
22273.969	1.6282	-1.818	Kurucz (1999)
22276.160	1.3036	-1.624	Kurucz (1999)
22277.008	1.1080	-2.197	Kurucz (1999)
22280.246	1.1036	-2.047	Kurucz (1999)
22285.527	1.1177	-2.225	Kurucz (1999)
22294.160	1.2609	-1.718	Kurucz (1999)
22295.695	1.1216	-2.042	Kurucz (1999)
22296.930	1.3900	-1.803	Kurucz (1999)
22299.426	1.4778	-1.853	Kurucz (1999)
22300.430	1.1397	-2.192	Kurucz (1999)
22301.910	1.4986	-1.856	Kurucz (1999)
22302.410	1.3260	-1.624	Kurucz (1999)
22309.961	1.2457	-1.718	Kurucz (1999)
22311.473	1.2942	-2.377	Kurucz (1999)

Table A2 – *continued*

Wavelength [Å]	EP [eV]	$\log gf$	Ref.
$^{12}C^{16}O$			
15594.223	0.1313	-7.7545	Goorvitch (1994)
15595.946	0.5118	-7.3273	Goorvitch (1994)
15597.348	0.1204	-7.7786	Goorvitch (1994)
15599.257	0.5339	-7.3121	Goorvitch (1994)
15600.737	0.1100	-7.8035	Goorvitch (1994)
15602.842	0.5564	-7.2971	Goorvitch (1994)
15604.392	0.1000	-7.8294	Goorvitch (1994)
15606.702	0.5794	-7.2822	Goorvitch (1994)
15608.312	0.0905	-7.8564	Goorvitch (1994)
15612.497	0.0814	-7.8841	Goorvitch (1994)
15615.250	0.6268	-7.2530	Goorvitch (1994)
15616.948	0.0729	-7.9133	Goorvitch (1994)
15619.940	0.6512	-7.2385	Goorvitch (1994)
15621.663	0.0648	-7.9439	Goorvitch (1994)
15624.908	0.6760	-7.2242	Goorvitch (1994)
15626.644	0.0572	-7.9755	Goorvitch (1994)
15630.155	0.7012	-7.2101	Goorvitch (1994)
15631.891	0.0500	-8.0092	Goorvitch (1994)
15635.682	0.7269	-7.1961	Goorvitch (1994)
15637.404	0.0434	-8.0446	Goorvitch (1994)
15641.490	0.7531	-7.1822	Goorvitch (1994)
15643.182	0.0372	-8.0824	Goorvitch (1994)
15647.580	0.7797	-7.1685	Goorvitch (1994)
15649.227	0.0314	-8.1226	Goorvitch (1994)
15653.953	0.8068	-7.1548	Goorvitch (1994)
15655.537	0.0262	-8.1659	Goorvitch (1994)
15660.610	0.8343	-7.1412	Goorvitch (1994)
15662.115	0.0214	-8.2128	Goorvitch (1994)
23554.786	0.0048	-6.4587	Goorvitch (1994)
23556.234	1.4594	-4.2830	Goorvitch (1994)
23558.269	0.8385	-4.5974	Goorvitch (1994)
23562.231	1.4886	-4.2734	Goorvitch (1994)
23564.307	0.8218	-4.6121	Goorvitch (1994)
23564.951	2.1495	-4.3503	Goorvitch (1994)
23568.674	1.5182	-4.2638	Goorvitch (1994)
23569.863	2.5598	-4.7140	Goorvitch (1994)
23570.723	0.2870	-5.5423	Goorvitch (1994)
23570.766	0.8056	-4.6271	Goorvitch (1994)
23575.563	1.5482	-4.2545	Goorvitch (1994)
23577.647	0.7898	-4.6424	Goorvitch (1994)
23577.693	0.0071	-6.3642	Goorvitch (1994)
23582.901	1.5786	-4.2451	Goorvitch (1994)
23582.995	2.1902	-4.3426	Goorvitch (1994)
23584.949	0.7744	-4.6582	Goorvitch (1994)
23587.982	0.2827	-5.5907	Goorvitch (1994)
23590.689	1.6095	-4.2359	Goorvitch (1994)
23592.672	0.7596	-4.6743	Goorvitch (1994)
23594.794	2.6067	-4.7071	Goorvitch (1994)
23598.928	1.6408	-4.2268	Goorvitch (1994)
23600.817	0.7451	-4.6908	Goorvitch (1994)
23601.032	0.0100	-6.2876	Goorvitch (1994)
23601.535	2.2314	-4.3350	Goorvitch (1994)
23605.665	0.2789	-5.6445	Goorvitch (1994)
23607.621	1.6725	-4.2177	Goorvitch (1994)
23609.383	0.7312	-4.7077	Goorvitch (1994)
23616.77	1.7047	-4.2088	Goorvitch (1994)
23618.369	0.7177	-4.7251	Goorvitch (1994)
23620.259	2.6541	-4.7001	Goorvitch (1994)
23620.571	2.2729	-4.3273	Goorvitch (1994)
23623.771	0.2756	-5.7051	Goorvitch (1994)
23624.802	0.0133	-6.2232	Goorvitch (1994)
23626.375	1.7373	-4.2000	Goorvitch (1994)
23627.778	0.7046	-4.7430	Goorvitch (1994)

Table A2 – *continued*

Wavelength (air) [Å]	*EP* [eV]	log *gf*	Ref.
23636.44	1.7703	-4.1912	Goorvitch (1994)
23637.608	0.6921	-4.7617	Goorvitch (1994)
23640.108	2.3148	-4.3198	Goorvitch (1994)
23642.301	0.2728	-5.7747	Goorvitch (1994)
23646.262	2.7018	-4.6931	Goorvitch (1994)
23646.967	1.8037	-4.1824	Goorvitch (1994)
23647.859	0.6799	-4.7807	Goorvitch (1994)
23649.006	0.0172	-6.1676	Goorvitch (1994)
$^{12}C^{17}O$			
23555.604	0.5678	-4.9176	Goorvitch (1994)
23558.862	0.0255	-5.9974	Goorvitch (1994)
23561.873	0.5513	-4.9326	Goorvitch (1994)
23568.546	0.5353	-4.9473	Goorvitch (1994)
23575.626	0.5198	-4.9630	Goorvitch (1994)
23583.110	0.5047	-4.9788	Goorvitch (1994)
23591.000	0.4901	-4.9948	Goorvitch (1994)
23599.294	0.4759	-5.0114	Goorvitch (1994)
23607.995	0.4621	-5.0284	Goorvitch (1994)
23617.100	0.4489	-5.0459	Goorvitch (1994)
23626.613	0.4360	-5.0639	Goorvitch (1994)
23636.530	0.4237	-5.0825	Goorvitch (1994)
23646.853	0.4117	-5.1016	Goorvitch (1994)
$^{12}C^{18}O$			
23556.518	0.2538	-5.4594	Goorvitch (1994)
23564.155	0.2389	-5.4752	Goorvitch (1994)
23572.184	0.2245	-5.4913	Goorvitch (1994)
23580.602	0.2105	-5.5079	Goorvitch (1994)
23589.412	0.1970	-5.5251	Goorvitch (1994)
23598.614	0.1839	-5.5426	Goorvitch (1994)
23608.206	0.1712	-5.5607	Goorvitch (1994)
23618.19	0.1590	-5.5792	Goorvitch (1994)
23628.565	0.1473	-5.5984	Goorvitch (1994)
23639.333	0.1360	-5.6182	Goorvitch (1994)
$^{13}C^{16}O$			
23560.596	1.3099	-4.9751	Goorvitch (1994)
23563.521	0.1719	-5.5580	Goorvitch (1994)
23570.753	1.3437	-4.9666	Goorvitch (1994)
23573.485	0.1596	-5.5766	Goorvitch (1994)
23581.341	1.3779	-4.9582	Goorvitch (1994)
23583.842	0.1478	-5.5957	Goorvitch (1994)
23592.363	1.4126	-4.9496	Goorvitch (1994)
23594.59	0.1365	-5.6156	Goorvitch (1994)
23603.818	1.4476	-4.9412	Goorvitch (1994)
23605.733	0.1256	-5.6360	Goorvitch (1994)
23615.711	1.4831	-4.9329	Goorvitch (1994)
23617.268	0.1151	-5.6574	Goorvitch (1994)
23628.043	1.5189	-4.9248	Goorvitch (1994)
23629.197	0.1051	-5.6794	Goorvitch (1994)
23640.814	1.5552	-4.9165	Goorvitch (1994)
23641.522	0.0956	-5.7025	Goorvitch (1994)
OH			
15593.563	0.8740	-5.358	Kurucz (1999)
15608.357	0.4942	-7.209	Kurucz (1999)
15609.683	0.4942	-7.209	Kurucz (1999)
15621.766	0.8374	-6.734	Kurucz (1999)
15624.434	0.8415	-7.006	Kurucz (1999)
15624.660	0.1336	-8.233	Kurucz (1999)
15626.704	0.5413	-5.198	Kurucz (1999)
15627.290	0.8871	-5.435	Kurucz (1999)
15627.293	0.8871	-5.435	Kurucz (1999)
15627.413	0.5413	-5.198	Kurucz (1999)
15628.902	0.1337	-8.233	Kurucz (1999)
15636.235	0.8876	-7.202	Kurucz (1999)
15636.596	0.8876	-7.202	Kurucz (1999)
15643.302	0.8420	-7.007	Kurucz (1999)
15650.557	0.8643	-5.587	Kurucz (1999)
15650.797	0.8643	-5.587	Kurucz (1999)
15651.896	0.5341	-5.132	Kurucz (1999)
15653.480	0.5343	-5.132	Kurucz (1999)
15654.116	0.8383	-6.734	Kurucz (1999)
15655.053	0.3041	-7.713	Kurucz (1999)
15658.127	0.3038	-7.713	Kurucz (1999)